Biophysical *Journal*
Article

Internal motion of chromatin fibers is governed by dynamics of uncompressed linker strands

Rajib Basak[1], William Rosencrans[2], Indresh Yadav[1], Peiyan Yan[1], Nikolay V. Berezhnoy[3], Qinming Chen[3], Jeroen A. van Kan[1], Lars Nordenskiöld[3], Anatoly Zinchenko[4], and Johan R. C. van der Maarel[1,*]

[1]Department of Physics, National University of Singapore, Singapore 117542, Republic of Singapore
[2]Eunice Kennedy Shriver National Institute of Child Health and Human Development, National Institutes of Health, Bethesda, MD, 20892-0924, USA
[3]School of Biological Sciences, Nanyang Technological University, Singapore 637551, Republic of Singapore
[4]Graduate School of Environmental Studies, Nagoya University, Furo-cho, Chikusa-ku, Nagoya 464-8601, Japan
[*]Correspondence: johanmaarel@gmail.com

ABSTRACT Chromatin compaction and internal motion are fundamental aspects of gene expression regulation. Here, we have investigated chromatin fibers comprising recombinant histone octamers reconstituted with double-stranded bacteriophage T4-DNA. The size of the fibers approaches the typical size of genomic topologically associated domains. Atomic force and fluorescence (correlation) microscopy have been used to assess the structural organization, histone-induced compaction, and internal motion. In particular, the fibers are stretched on arrays of nanochannels, each channel with a diameter of 60 or 125 nm. Major intra-fiber segregation and fast internal fluctuations are observed. Full compaction was only achieved by triggering an attractive nucleosome interaction through the addition of magnesium cations. Besides compaction, histone complexation results in a dramatic decrease in the fiber's relaxation time. The relaxation times are similar to those of naked DNA with a comparable stretch, which indicates that internal motion is governed by the dynamics of uncompressed linker strands. Furthermore, the main reorganization process is association-dissociation of individually compacted regions. We surmise that the modulation of chromatin's internal motion by histone complexation might have implications for transcriptional bursting.

SIGNIFICANCE A major question in biology is how the eukaryotic genome can be compacted to such a high degree while preserving its accessibility to the machinery of life. An important aspect is the compaction of DNA into a chromatin fiber with the help of histone proteins through a hierarchy of largely unknown structures. Here, we show with a unique methodology and a relevant model system, that, besides being highly compacted, the chromatin fiber continuously folds and unfolds in more and less open configurations. We surmise that this previously largely overlooked fast internal motion has important implications for protein target search and associated biological processes such as DNA replication and repair as well as gene expression regulation.

INTRODUCTION

Understanding folding and compaction of DNA is important in biology as well as biotechnology. At its most basic unit, 147 base pairs of negatively charged DNA are wrapped around a positively charged histone octamer (HO) (1, 2). The histone octamer is made of two copies of four different histone proteins (H2A, H2B, H3, H4). The full fiber of DNA and histone octamers is known as the nucleosome core particle (NCP) and carries a net negative charge. NCPs are connected by a variable length of linker DNA and, together with H1 linker histone forms chromatin. Chromatin is further folded through a series of hierarchic, but largely unknown structures into the chromosome. As a result of this folding process, about two meters of human DNA is accommodated inside a micron-sized cell nucleus. Yet, through this compaction DNA remains highly accessible by the machinery of life. One of the major questions in biology is determining the mechanisms behind this apparent paradox. Folding of chromatin and, hence, DNA metabolism is controlled by DNA-histone and histone-histone interactions, which are modulated by various biophysical and biochemical remodeling mechanisms.

The higher order structures of chromatin have not been conclusively determined. Chromatin was long thought to be arranged in a regular 30 nm fiber (3, 4). More recently, it has been suggested that chromatin is folded into a rather disordered, highly dynamic structure (5–9). *In vivo*, larger regions of chromatin loosely exist in topologically associating domains (TADs). TADs with a typical size of about 250

nm contain DNA segments of mega-base length, in which base pair sequences preferentially interact with one another (10, 11). While many studies have addressed the structure and dynamics of smaller segments of chromatin (12, 13), only a few have focused on larger chromatins that provide a good model system for TADs. Here, we will use reconstituted chromatin by complexation of over-expressed, refolded, and purified histone octamer on bacteriophage T4-DNA (165.6 kbp) (14–16). This system can serve as a model of (smaller) TADs, since it approaches their molecular weight, there are no preferential histone binding sites, and the flexibility in nucleosome position is generally conserved *in vivo* human chromatin (17). Additional advantages of reconstituted chromatin are the uniform length of the DNA molecule and the possibility to control the stoichiometry of histone complexation. Our model system lacks linker histone H1 to avoid complications regarding heterogeneity and to avoid fixated structures. Nevertheless, this reduced chromatin system is still highly relevant to the *in vivo* situation, because the viability of cells is tolerant to depletion of H1 and lower eukaryotes (*e.g.*, yeast) show little change in transcription profile and phenotype after complete knockout of the linker histone (18).

A relatively novel single-molecule manipulation technology is based on a platform of nanofluidic channels. These channels are quasi one-dimensional with rectangular cross-sections with a diameter of a few tens to hundreds of nanometers. They have extensively been used before to study DNA and DNA-ligand interactions (19–23). Chromatin has also previously been stretched by confinement to a nanochannel, mainly for analysis of the epigenome (24, 25). Nanofluidic studies on reconstituted bacteriophage λ-DNA have shown a moderate two-fold compaction with respect to bare DNA but this might depend on channel geometry, histone loading, and other remodeling factors such as buffer composition and the presence of divalent cations (26). Another important application of the nanofluidic system is the possibility to study chromatin's internal motion, that is, the timing of internal density fluctuations, from analysis of fluorescence correlation (27). This is particularly relevant from a biological point of view, because the cross-sectional diameter of the channels (125 nm or less) is around the size of TADs and TAD dynamics might play a role in transcriptional bursting (28, 29). Here, we will use nanofluidics in combination with fluorescence (correlation) microscopy to investigate compaction and internal motion of TAD-like reconstituted chromatin and how these are related to histone complexation.

MATERIALS AND METHODS

Sample preparation

T4GT7 DNA was purchased from Nippon Gene, Japan and dissolved to a concentration of 0.7 μg of nucleotides/mL in Tris-EDTA-KCl buffer (10 mM KCl, 10 mM Tris-HCl, 1 mM EDTA, pH = 7.8). The coding sequences of recombinant human core histones were cloned in the pET21a (H2A, H2B and H3) and pET3a (H4) vectors. Each core histone was individually expressed in the *Escherichia coli* BL21(DE3)-pLysS strain. Histone octamers (HOs) were refolded from an equimolar mixture of the core histones, purified using size-exclusion chromatography, and assessed with SDS-PAGE chromatography (30). Chromatin reconstitution from T4-DNA and HO was done following the salt dialysis procedure (14, 31, 32). Chromatins with two degrees of HO loading were prepared with 1 HO per 200 (100% HO-loading) and 400 (50% HO-loading) bps of DNA, respectively. Solution of naked T4-DNA in the same buffer was also prepared. The final concentration of all samples is 0.3 mg of DNA/L and the final buffer comprises 10 mM Tris-HCl (pH = 7.5), 1 mM EDTA, 10 mM NaCl, 1mM DTT, and various amounts of $MgCl_2$. Prior to fluorescence imaging, DNA was stained with YOYO-1 (Invitrogen, Carlsbad, CA) at a ratio of one dye molecule for each four base pairs.

Chip fabrication

Nanofluidic devices were fabricated by replication in polydimethylsiloxane with enhanced elasticity modulus (X-PDMS) of patterned master stamps (33–35). The device layout consisted of an array of 90 μm long, rectangular channels with a cross-section of 50×70 nm^2 (60-nm channel system) or 120×130 nm^2 (125-nm system) and uncertainty in width and depth of ±5 nm.The nanochannel part of the stamps was made in hydrogen silsesquioxane (HSQ) resist (Dow Corning, Midland, MI) using a lithography process with proton beam writing. The array of nanochannels is connected to two loading reservoirs through a superposing v-shaped set of microchannels made in mr-DWL photoresist (Micro Resist Technology, Berlin, Germany) with a laser writer (Heidelberg micro PG 101). The heights and widths of the ridges in the master stamp were measured with atomic force microscopy (Bruker Dimension Icon, Billerica, MA) and scanning electron microscopy (JEOL JSM6700F), respectively. The master stamp was coated with diamond-like-carbon layer before being copied in the inorganic-organic hybrid polymer OrmoStamp (Micro Resist Technology). After copying, the stamp was coated with a 5-nm-thick carbon layer to ensure perfect release of the replicated chips. The stamp was replicated in X-PDMS by spin coating and followed by curing at 333 K for 24h. Following plasma oxidation (Harrick, Ossining, NY), the X-PDMS replicas were sealed with a glass coverslip.

Fluorescence imaging

The YOYO stained chromatin was pipetted into the two loading reservoirs connected to the array of nanochannels. The fibers were subsequently driven into the channels by electrophoresis. For this purpose, two platinum electrodes were immersed in the reservoirs and connected to a power supply with a voltage in the range 0.1–20 V (Keithley, Cleveland, Ohio). Once the

fibers were brought inside the nanochannels, the electric field was switched off and the molecules were allowed to relax to their equilibrium state for at least 60 s. The stained fibers were visualized with a Nikon Eclipse Ti inverted fluorescence microscope equipped with a diode laser (200 mW/488 nm, (Omicron, Germany), filter set, and a 100× oil immersion objective (numerical aperture 1.49). Movie clips of typically 2 min duration at a rate of 20 frames/s were recorded with an electron-multiplying charged coupled device camera (Andor iXon X3). The image pixel size of 0.16×0.16 μm^2 was calibrated with the help of a metric ruler. The clips were analyzed using home-developed scripts in MATLAB, R2020a (MathWorks, Natick, MA).

Atomic force microscopy

A 5 μL droplet of reconstituted T4-chromatin was spotted onto a plasma-oxidized silica surface. After 10 min to allow for DNA adsorption onto the surface, the specimens were developed by flushing them with 1 mL of ultra-pure water followed by drying in a stream of N_2 gas. Atomic force imaging was done with the Dimension Icon microscope at room temperature in air. Images were acquired in the tapping mode with silicon (Si) cantilevers (spring constant of 19–55 N/m) and operated below their resonance frequency (typically 270–370 kHz). The images were flattened, and the contrast and brightness were adjusted for optimal viewing conditions.

RESULTS AND DISCUSSION

Atomic Force Microscopy

Chromatin was prepared by reconstitution of bacteriophage T4-DNA and over-expressed, refolded, and purified histone octamer (HO) (30). As established and confirmed in earlier work by Atomic Force Microscopy (AFM), Transmission Electron Microscopy (TEM), and gel assays, this reconstitution with T4-DNA results in the formation of nucleosomes and chromatin (14). The stoichiometric ratios employed in the reconstitution procedure are one HO per 400 bps (50% HO-loading) and one per 200 bps (100% HO-loading), respectively. In particular, gel assays showed that the fibers with 100% HO-loading are protected against digestion with micrococcal nuclease. We first further analyzed the fibers with tapping mode atomic force microscopy. Characteristic images pertaining to 50% and 100% HO-loading are shown in Figure 1 and S1. Reconstitution is confirmed by the appearance of the beads on a string hallmark resulting from the formation of nucleosomes. The arrangement of the nucleosomes along the DNA is heterogeneous with some sections more densely complexed with HO than other sections. This heterogeneity is plausibly caused by interaction among the nucleosomes. In the case of DNA with 50% HO-loading the overall density of the nucleosomes is lower and there are large sections of naked DNA. No clear 30-nm fiber or any other regularly repeating arrangement of the nucleosomes along DNA was observed.

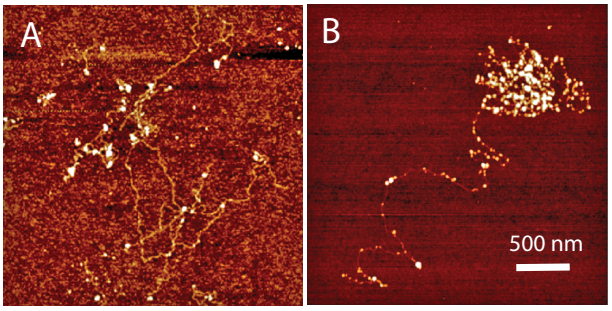

Figure 1: **(A)** Tapping mode atomic force microscopy image of reconstituted chromatin, that is T4-DNA with 1 HO per 400 bps (50% HO-loading). **(B)** As in panel (A) but with 1 HO per 200 bps (100% HO-loading).

At a larger scale and for 100% HO loading in particular, the chromatin is clustered in a web-like structure. This clustering is plausibly mediated by nucleosome interaction. In the case of 50% HO loading, nucleosome clustering is still observed albeit to lesser degree and smaller regions due to the sparser distribution of nucleosomes. The structure of the reconstituted chromatin appears to be rather inhomogeneous, both in terms of the distribution of the bound HO along the DNA as well as clustering of the nucleosomes at a larger scale. As we will see shortly, the inhomogeneous distribution of the nucleosomes results in inhomogeneous compaction and internal association-dissociation dynamics.

Nanofluidic stretching

Compaction was followed by monitoring the stretch of the fibers confined to a nanochannel with fluorescence microscopy. DNA was stained through binding of YOYO-1 with a ratio of one dye per 4 bps. The dye was added to the reconstituted fibers just prior to the imaging experiment. It was checked that with a reduction of the staining level from one dye per 4 to 50 bps the stretch of the reconstituted fibers decreased by 5%. This marginal decrease is consistent with previous experiments showing that labeling with YOYO-1 at a ratio of 1:10 does not significantly affect the assembly reaction and that ethidium bromide intercalator induces less than 5% dissociation of nucleosomes up to 0.15 dye per bp (36, 37). The decrease in stretch of the fiber following reduction of the staining level of one dye per 4 to 50 bps is plausibly related to a decrease in contour length of the linker strands. Furthermore, it should be noted that the binding of the YOYO-1 dye on DNA is largely dependent on the ionic strength of the supporting buffer medium. At the employed buffer composition of 10 mM Tris-HCl, 10 mM NaCl, and 1 mM EDTA the DNA molecules are clearly discernible. However, the reduced binding of the intercalating dye at higher ionic strengths precludes accurate fluorescence imaging of DNA in physiological saline conditions.

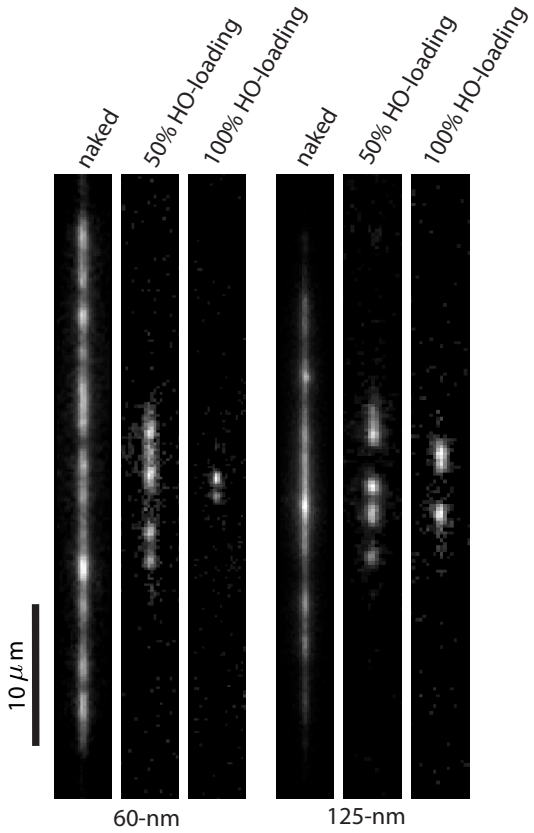

Figure 2: Fluorescence still images of naked T4-DNA and T4-DNA with 50% and 100% HO-loading stretched in the 60-nm and 125-nm channel systems.

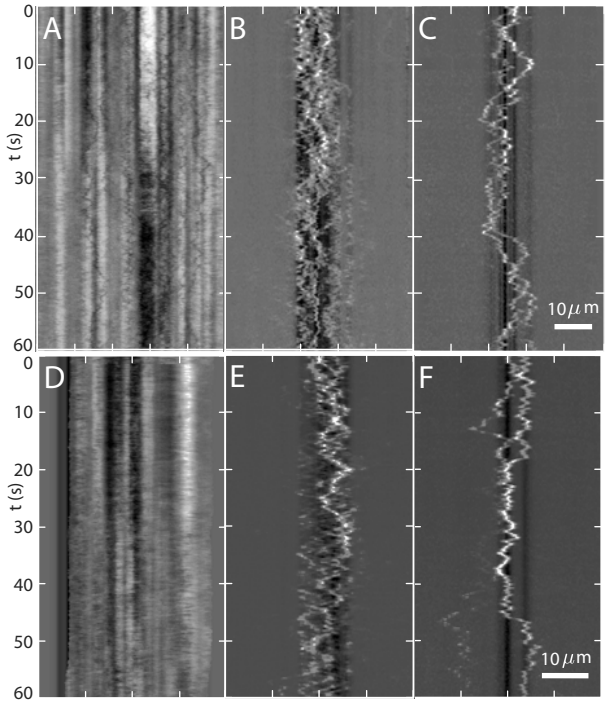

Figure 3: **(A–C)** Kymograph of density fluctuation $\delta\rho(z,t)$ for naked T4-DNA (A) and T4-DNA with 50% HO-loading (B) and 100% HO-loading (C) stretched in the 60-nm channel system. **(D-F)** As in panels (A-C) but for the 125-nm system.

Naked T4-DNA as well as the fibers were brought into arrays of 90 μm long, rectangular channels with a cross-section of 50×70 nm^2 (60-nm channel system) and 120×130 nm^2 (125-nm system) by electrophoresis. After switching off the electric field, the molecules relax to their equilibrium state within 60 s. Video recording was started 2–5 min after the molecules were brought into the channels. Video clips are shown in Supplementary Movies 1–6. Still images from the clips are displayed in Figure 2. No significant sticking of the chromatin fibres to the channel substrate or coverslip was observed. Qualitatively, the same behavior is observed in the 60-nm and 125-nm channel systems. With increasing HO-loading, the DNA molecules are progressively compacted. The fibers take on the appearance of bright blobs, each stretched to a few micrometer and connected by barely visible strands of uncompressed DNA. Furthermore, these blobs continuously reform and stochastically associate and dissociate, so that the fibers fluctuate between relatively more and less open configurations. As will be shown below, this fluctuation is largely suppressed following the addition of Mg^{2+} cations. Naked DNA does not show intramolecular segregation, although its internal motion is considerably slowed down (see below).

In order to visualize DNA density fluctuations, the clips were analyzed by obtaining the z-axis projected intensity profile $\rho(z,t)$ along the channel for each frame. Effects of photobleaching were corrected by normalization of each frame's intensity profile to its total intensity. The time-averaged profile $\bar{\rho}(z)$ was obtained by averaging over the duration of the clip. A profile of intensity *fluctuation* was then obtained by subtraction of the time-averaged intensity profile from the temporal profile, that is, $\delta\rho(z,t) = \rho(z,t) - \bar{\rho}(z)$. Examples of thus obtained kymographs pertaining to naked T4-DNA as well as reconstituted chromatin with 50% and 100% HO-loading in the 60-nm and 125-nm channel systems are shown in Figure 3. With the assumption that the intensity is proportional to DNA density, these kymographs represent density fluctuation $\delta\rho(z,t)$. The kymographs demonstrate very slow fluctuations on a time scale of seconds in the density of naked DNA. With increasing HO-loading, the density fluctuates over a smaller range and becomes increasingly coarse-grained.

Chromatin internal dynamics will be further discussed below. First, the various fibers are characterized by their time-averaged stretch $L_\parallel$ along the channel. For each frame (time t), we determined the z-axis projected second moment according to $S(t) = \int \rho(z,t)(z-z_{cm})^2 dz$ with center of mass $z_{cm} = \int \rho(z,t) z dz$. The time-averaged stretch is then given by $L_\parallel^2 = 12\,\langle S(t)\rangle$, where the chevrons denote an average

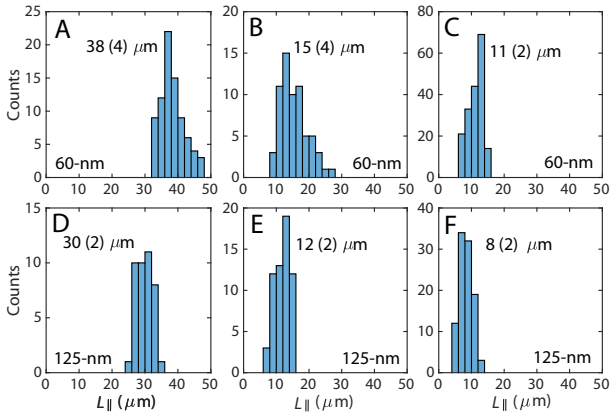

Figure 4: **(A–C)** Distribution in time-averaged stretch $L_{\parallel}$ of naked T4-DNA (A) and T4-DNA with 50% HO-loading (B) and 100% HO-loading (C) as obtained from the second moment of the fluorescence intensity profile in the 60-nm channel system. **(D-F)** As in panels (A-C) but for the 125-nm channel system. Mean values and standard deviations (bracketed) pertaining to the width of the distributions are indicated.

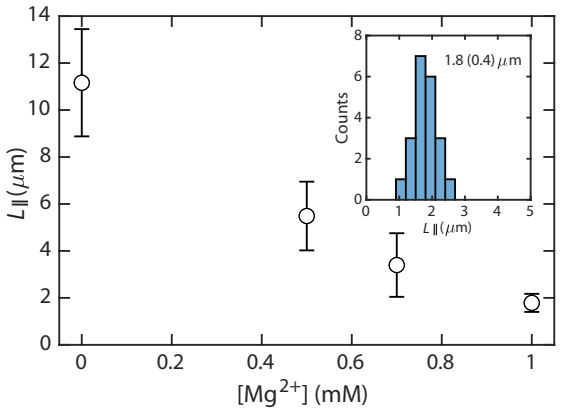

Figure 5: Time-averaged stretch $L_{\parallel}$ of T4-DNA with 100% HO-loading in the 60-nm channel system vs Mg^{2+} cation concentration. The inset shows the distribution in stretch in the presence of 1 mM Mg^{2+}.

over all frames (1 min clips). Distributions of the stretch, mean values, and standard deviations pertaining to the width of the distributions are shown in Figure 4. Results obtained from the 60-nm and 125-nm channel systems are qualitatively similar, but the molecules are stretched to a larger extent in the narrower channel due to stronger confinement. This is most pronounced for naked DNA, for the reconstituted fibers the shifts are marginal. Note that the fibers are non-uniformly stretched, so that these time-averaged results bear little significance for profiling applications based on mapping of fluorescence markers.

The maximal stretch of naked DNA is 52% and 41% of its stained contour length of ~73 μm in the 60-nm and 125-nm channel system respectively. The stained persistence length is ~60 nm (38). With a cross-sectional diameter of 1–2 times the persistence length, the molecules are in the blob-to-deflection transition regime (39). In the wider 125 nm channel, DNA is still coiled and the distribution in stretch is close to Gaussian. In the narrower 60 nm channel, the molecules are undulating and deflected from the wall. The corresponding distribution in stretch is asymmetrically tapered towards lower values with respect to its maximal stretch due to back-folding and the formation of hairpins (40–43). A discussion of the latter effects is beyond the scope of the present contribution. Reconstituted chromatin is progressively compacted as shown by a fourfold decrease in stretch with increasing HO-loading. Yet, they do not achieve a fully compacted state, because of the fluctuation between relatively more and less open configurations. The corresponding distributions in stretch are rather wide, which is most probably related to variation in HO complexation. With a maximal HO loading of 100% (HO to bps ratio of 1:200), 147 bps per nucleosome, and assuming that all HO are bound on DNA, the total length of the linker strands is about 27% of the total contour length of the DNA molecule. The concomitant fourfold decrease in stretch indicates that the stretch of the fibers is mainly determined by the uncompressed linker strands with a minor contribution from compacted regions.

Chromatin compaction is attributed to attractive nucleosome-nucleosome interaction, among others through histone tail bridging and multivalent ion correlation effects (44–46). Compaction of reconstituted chromatin in the bulk phase with the help of Mg^{2+} cations has previously been demonstrated (14). Here, we have monitored the stretch of the 100% HO-loaded fiber confined to a 60 nm channel for a series of Mg^{2+} concentrations. With increasing Mg^{2+} cation concentration, the fluctuation between open and closed configurations as indicated by the appearance of bright blobs is progressively suppressed. Concurrently, the time-averaged stretch gradually decreases until it becomes ~2 μm at 1 mM Mg^{2+} (Figure 5). Compaction of the same fiber in the bulk phase requires an order of magnitude higher concentration of ~10 mM Mg^{2+} (14). As in the case for naked DNA in the presence of condensing agents or ligands, compaction into a condensed state is facilitated by confinement to a nanospace (19). This observation suggests that the compaction is mediated by condensation of the uncompressed linker strands besides multivalent ion-induced nucleosome interaction. Our results confirm that for high resolution mapping of histone states channels with a cross-sectional diameter of less than 30 nm are required (24).

Internal Motion

In the absence of divalent cations, the reconstituted chromatin fibers fluctuate between relatively more and less open config-

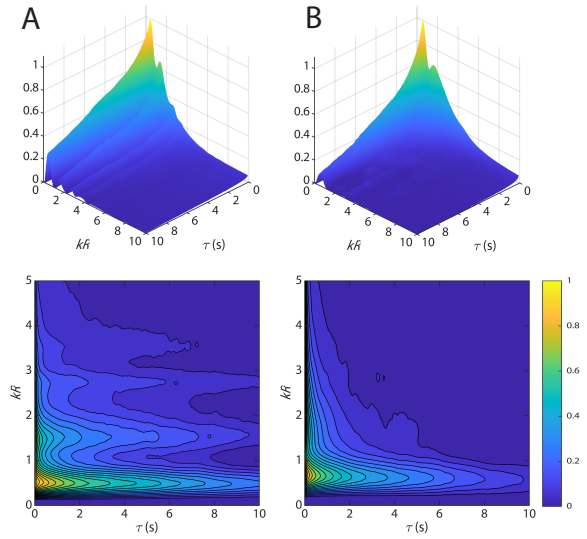

Figure 6: **(A)** Surface (top) and contour (bottom) plots of the intermediate dynamic structure factor $F(k,\tau)$ of T4-DNA with 50% HO-loading confined to a 60 nm channel. **(B)** As in panel (A) but for 100% HO-loading. Notice that the k axis has been scaled by multiplication with half wavelength of the fundamental R.

urations. This fluctuation is possibly related to association-dissociation dynamics of different compacted regions, folding and unfolding dynamics, and/or nucleosome relocation dynamics. In order to obtain more insight in the nature of this fluctuation, we have investigated DNA internal motion through analysis of fluorescence correlation. The intermediate dynamic structure factors $F(k,\tau)$, as a function of spatial wavenumber k and lag-time τ, were obtained from the kymographs of the density fluctuation following a previously reported procedure (27). Results pertaining to an average of 80 and 45 chromatin fibers with 50% and 100% HO-loading, respectively, confined to a 60 nm channel, are displayed in Figure 6. The result for an average of 45 fibers with 100% HO-loading in the 125-nm channel system is shown in Figure S2. There are no qualitative differences between the respective results obtained in the two channel systems. In the case of the fully compacted fiber in the presence of 1 mM Mg^{2+}, $F(k,\tau)$ shows a very fast initial decay within a lag-time, which is due to the autocorrelation of the camera's shot noise. Accordingly, for fully compacted DNA, accurate information regarding internal motion could not be obtained.

Intramolecular hydrodynamic interaction is screened beyond a distance scale of around the channel diameter. Uniformly stretched DNA inside a channel can then be considered a linear sequence of freely drained beads connected by springs and its dynamics can be described by the Rouse model in one dimension (27). The predominant features of $F(k,\tau)$ are odd Rouse modes associated with end-to-end fluctuation

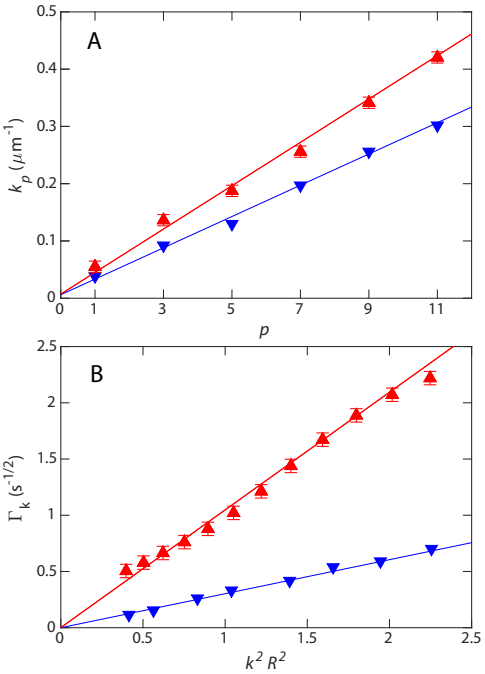

Figure 7: **(A)** Positions of the maxima k_p vs mode number p for T4-DNA with 50% (▽, blue) and 100% (△, red) HO-loading inside 60 nm channel. The solid lines denote linear fits giving the half wavelength of the fundamental R. **(B)** As in panel (A), but for the decay constants Γ_k vs k^2R^2 resulting from a fit of a stretched exponential to the initial decay of $F(k,\tau)$. The solid lines represent a linear fit with optimized Rouse relaxation times τ_R. Error margins for 50% HO-loading data are the same size of the symbols.

at positions $k_p = p/(2R)$ with mode number p and half wavelength of the fundamental R. Furthermore, $F(k,\tau)$ exhibits typical stretched exponential relaxation behavior with stretching exponent $1/2$. The molecular relaxation time, that is Rouse time τ_R, shows a cubic dependence on the stretch and, hence, molecular weight [the stretch is proportional to molecular weight for uniformly stretched DNA (47)]. Measured values of τ_R pertaining to various naked DNAs in the 125-nm channel system are collected in Table 1. Obtaining accurate values of τ_R for long DNAs confined to a 60 nm channel is challenging due to the considerable slowing down of intramolecular fluctuations. For naked T4-DNA inside a 60 nm channel, $F(k,\tau)$ does not appreciably relax within the relevant range of lag-times of a few seconds. We could only obtain an accurate value of τ_R for shorter, naked λ-DNA and careful selection of those molecules that are fully stretched as judged from the fluorescence intensity profile. The corresponding result is also collected in Table 1. For uniformly stretched, naked DNA molecules inside the 125 nm channel, the relaxation time is seen to increase by two orders of magnitude from tens of ms to a few s with increased stretch from

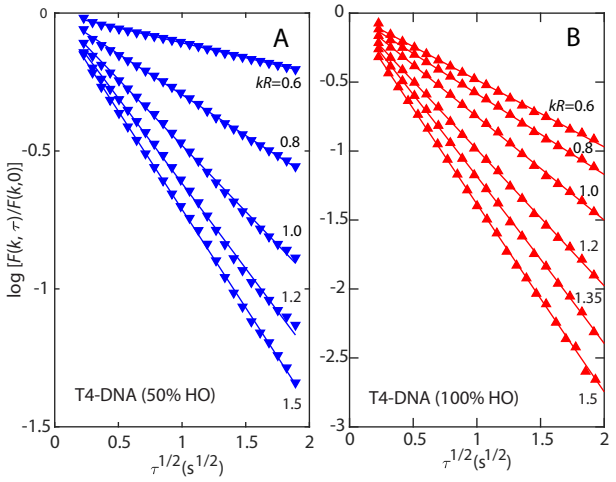

Figure 8: **(A)** $\log[F(k,\tau)/F(k,0)]$ vs $\tau^{1/2}$ for T4-DNA with 50% HO-loading inside 60 nm channel and indicated values of kR. The solid lines denote a stretched exponential fit. **(B)** As in panel (A) but for 100% HO-loading. Error margins are the same size of the symbols.

about 11 μm to 40 μm. With decreasing channel diameter, τ_R of λ-DNA is seen to decrease from ~60 ms to ~35 ms. This reduction in relaxation time is plausibly related to a decrease in hydrodynamic friction associated with increased alignment of the DNA segments following the transition from the blob to the deflection regime (20).

The reconstituted chromatin fibers are not uniformly stretched and show segregation between more and less compacted regions. Yet, odd Rouse modes associated with end-to-end fluctuation are still discernible in $F(k,\tau)$, although they are not particularly well resolved (see Figures 6 and S2). The poor mode resolution is plausibly caused by the distribution in time-averaged stretch (Figure 4). Nevertheless, the positions of the modes can be measured and their values are set out in Figure 7A and S3A for fibers confined to 60 and 125 nm channels, respectively. The presence of odd modes is confirmed by linear least-squares fits intersecting the origin. The half wavelengths of the fundamental and their standard deviations resulting from linear regression are collected in Table 1. Note that the fitted values of R are in reasonable agreement with the mean values of the stretch as obtained from the fluorescence intensity profiles.

Table 1: Dye-corrected contour length L, half wavelength of the fundamental R, and relaxation time τ_R of various DNAs and their fibers in 60-nm and 125-nm channel systems

		L (μm)	R (μm)	τ_R (ms)
60 nm				
T4-DNA	100% HO	73.1	12.8±0.2	30±5
T4-DNA	50% HO	73.1	17.4±0.4	350±50
λ-DNA	naked	21.4	14.6±0.3	35±4
125 nm				
T4-DNA	100% HO	73.1	11.3±0.2	22±4
λ-DNA[a]	naked	21.4	11.3±0.1	60±5
λ-DNA$_2$[a]	naked	42.8	22.7±0.2	560±60
λ-DNA$_3$[a]	naked	64.2	29.9±0.6	1800±300
T4-DNA	naked	73.1	39.8±0.8	2600±600

[a] Ref. (27)

With increasing lag-time, $F(k,\tau)$ is seen to decay with a faster rate with 100% HO-loading (60-nm channel system, Figure 6). This indicates a further increase in internal motion with increasing HO complexation. In the case of Rouse dynamics at shorter times, $F(k,\tau)$ decays as a stretched exponential, that is,

$$F(k,\tau) = F(k,0)\exp\left(-\Gamma_k \tau^{1/2}\right), \tag{1}$$

with decay constant (27, 48, 49)

$$\Gamma_k = k^2R^2/(\pi^{3/2}\tau_R^{1/2}). \tag{2}$$

A stretched exponential was fitted to the initial decay for kR values in the range $0.6 < kR < 1.6$ with nonlinear least-squares regression. For larger values of kR, the fits become unreliable due to poorer statistics. Furthermore, $F(k,\tau)$ shows a very fast decay over a lag-time due to camera noise. The corresponding data points were excluded from the fits. Results of the fits pertaining to fibers with 50% and 100% HO-loading, respectively, and in the 60-nm channel system are displayed in Figure 8. The result for fibers with 100% HO-loading confined to a 125-nm channel is shown in Figure S4. Irrespective of the channel diameter and HO-loading percentage, perfect stretched exponential behavior with a stretched exponent of 1/2 is observed. The corresponding fitted values of Γ_k vs k^2R^2 are shown in Figure 7B and S3B, respectively. Origin intersecting, linear dependencies are observed. Rouse relaxation times and standard deviations as obtained from linear regression analysis are also collected in Table 1.

With increasing degree of complexation, the relaxation time pertaining to internal density fluctuations decreases from several seconds for naked DNA, through several hundred ms for 50% HO loading, to a few tens of ms for 100% HO loading. These two orders of magnitude decease in τ_R shows that, besides compaction, HO complexation results in a dramatic increase in internal motion. The values of τ_R for the reconstituted fibers are of the same order of magnitude as those of naked DNAs with a comparable stretch. This shows that besides the stretch, chromatin's internal motion is governed by the uncompressed linker strands. Increased complexation results in shorter linker strands with less hydrodynamic friction and, hence, faster internal motion. The fluctuation in stretch can then be interpreted in terms of association-dissociation dynamics of different, individually compacted regions. Other reorganization processes such as folding and unfolding within

the compacted regions themselves play a less dominant role but cannot be excluded. The marginal difference in relaxation time for the fibers with 100% HO loading in the 60 and 125-nm channel systems is plausibly related to confinement-induced changes in stretch and friction of the linker strands.

CONCLUSION

With a view to gain insight in chromatin's compaction and internal motion, we have investigated a well-defined TAD-like model system of histone-loaded DNA. Reconstitution is confirmed with atomic force microscopy. The structure of the reconstituted fibers appears to be rather inhomogeneous, both in terms of the distribution of bound histones along the DNA as well as clustering of the nucleosomes at a larger scale. The fibers were stretched on an array of nanochannels, each channel with a cross-sectional diameter of about one or two times the bare DNA's persistence length, and visualized with fluorescence microscopy. A striking observation is intra-fiber segregation and relatively fast internal motion between more and less open configurations in the prevalent buffer condition. Full compaction was only achieved by triggering an attractive nucleosome-nucleosome interaction through the addition of divalent magnesium cations. The final compacted size is $\sim$2 μm (a factor of $\sim$15). Such a stretch might not be sufficient for high resolution mapping of histone states, which requires almost full linearisation (>95%) in a channel with a cross-section of less than 100 nm^2 (24, 50). Fluorescence autocorrelation shows predominant odd order modes associated with end-to-end fluctuation and typical stretched exponential relaxation behavior with stretching exponent $1/2$ pertaining to Rouse dynamics. The derived molecular relaxation time decreases by two orders of magnitude from several seconds for naked DNA to a few tens of ms for the ones with 100% histone loading. Complexation by histones, hence, results in a dramatic increase in internal motion. The internal fluctuations cannot be significantly affected by sliding of histones over kbps distances along DNA, since this occurs on a much longer time scale of seconds to minutes (51). The similarity in relaxation time between the fibers and naked DNA's with a comparable stretch indicates that the internal motion is governed by dynamics of uncompressed linker strands. Furthermore, the main observed reorganization process is association-dissociation of various individually compacted regions of the complex. Folding and unfolding within the compacted regions themselves play a less dominant role but cannot be excluded. We surmise that the modulation of chromatin's internal motion by the degree of histone complexation might have implications for understanding transcriptional bursting.

AUTHOR CONTRIBUTIONS

LN, AZ, JAvK, and JRCvdM designed research. RB, WR, IY, and JRCvdM carried out research and analyzed the data. PY, NVB, and QC provided reagents. JRCvdM wrote the article.

ACKNOWLEDGMENTS

This work was supported by Ministry of Education, Singapore (MOE) Academic Research Fund Tier 1 Grant (2018-T1-001-114).

REFERENCES

1. Luger, K., A. W. Mäder, R. K. Richmond, D. F. Sargent, and T. J. Richmond, 1997. Crystal structure of the nucleosome core particle at 2.8 Å resolution. *Nature* 389:251–260.

2. Davey, C. A., D. F. Sargent, K. Luger, A. W. Maeder, and T. J. Richmond, 2002. Solvent mediated interactions in the structure of the nucleosome core particle at 1.9 Å resolution. *J. Mol. Biol.* 319:1097–1113.

3. Finch, J., and A. Klug, 1976. Solenoidal model for superstructure in chromatin. *Proc. Natl. Acad. Sci. U. S. A.* 73:1897–1901.

4. Song, F., P. Chen, D. Sun, M. Wang, L. Dong, D. Liang, R.-M. Xu, P. Zhu, and G. Li, 2014. Cryo-EM study of the chromatin fiber reveals a double helix twisted by tetranucleosomal units. *Science* 344:376–380.

5. Maeshima, K., S. Ide, K. Hibino, and M. Sasai, 2016. Liquid-like behavior of chromatin. *Curr. Opin. Genet. Dev.* 37:36–45.

6. Ashwin, S., T. Nozaki, K. Maeshima, and M. Sasai, 2019. Organization of fast and slow chromatin revealed by single-nucleosome dynamics. *Proc. Natl. Acad. Sci. U. S. A.* 116:19939–19944.

7. Eltsov, M., K. M. MacLellan, K. Maeshima, A. S. Frangakis, and J. Dubochet, 2008. Analysis of cryo-electron microscopy images does not support the existence of 30-nm chromatin fibers in mitotic chromosomes in situ. *Proc. Natl. Acad. Sci. U. S. A.* 105:19732–19737.

8. Nishino, Y., M. Eltsov, Y. Joti, K. Ito, H. Takata, Y. Takahashi, S. Hihara, A. S. Frangakis, N. Imamoto, T. Ishikawa, et al., 2012. Human mitotic chromosomes consist predominantly of irregularly folded nucleosome fibres without a 30-nm chromatin structure. *EMBO J.* 31:1644–1653.

9. Joti, Y., T. Hikima, Y. Nishino, F. Kamada, S. Hihara, H. Takata, T. Ishikawa, and K. Maeshima, 2012. Chromosomes without a 30-nm chromatin fiber. *Nucleus* 3:404–410.

10. Dixon, J. R., S. Selvaraj, F. Yue, A. Kim, Y. Li, Y. Shen, M. Hu, J. S. Liu, and B. Ren, 2012. Topological domains in mammalian genomes identified by analysis of chromatin interactions. *Nature* 485:376–380.

11. Pope, B. D., T. Ryba, V. Dileep, F. Yue, W. Wu, O. Denas, D. L. Vera, Y. Wang, R. S. Hansen, T. K. Canfield, et al., 2014. Topologically associating domains are stable units of replication-timing regulation. *Nature* 515:402–405.

12. Meng, H., K. Andresen, and J. Van Noort, 2015. Quantitative analysis of single-molecule force spectroscopy on folded chromatin fibers. *Nucleic Acids Res.* 43:3578–3590.

13. Kaczmarczyk, A., A. Allahverdi, T. B. Brouwer, L. Nordenskiöld, N. H. Dekker, and J. Van Noort, 2017. Single-molecule force spectroscopy on histone H4 tail-cross-linked chromatin reveals fiber folding. *J. Biol. Chem.* 292:17506–17513.

14. Zinchenko, A., N. V. Berezhnoy, S. Wang, W. M. Rosencrans, N. Korolev, J. R. C. van der Maarel, and L. Nordenskiöld, 2018. Single-molecule compaction of megabase-long chromatin molecules by multivalent cations. *Nucleic Acids Res.* 46:635–649.

15. Zinchenko, A., N. V. Berezhnoy, Q. Chen, and L. Nordenskiöld, 2018. Compaction of single-molecule megabase-long chromatin under the influence of macromolecular crowding. *Biophys. J.* 114:2326–2335.

16. Zinchenko, A., Q. Chen, N. V. Berezhnoy, S. Wang, and L. Nordenskiöld, 2020. Compaction and self-association of megabase-sized chromatin are induced by anionic protein crowding. *Soft Matter* 16:4366–4372.

17. Valouev, A., S. M. Johnson, S. D. Boyd, C. L. Smith, A. Z. Fire, and A. Sidow, 2011. Determinants of nucleosome organization in primary human cells. *Nature* 474:516–520.

18. Woodcock, C. L., A. I. Skoultchi, and Y. Fan, 2006. Role of linker histone in chromatin structure and function: H1 stoichiometry and nucleosome repeat length. *Chromosome Res.* 14:17–25.

19. van der Maarel, J. R. C., C. Zhang, and J. A. van Kan, 2014. A nanochannel platform for single DNA studies: from crowding, protein DNA interaction, to sequencing of genomic information. *Isr. J. Chem.* 54:1573–1588.

20. Reisner, W., J. N. Pedersen, and R. H. Austin, 2012. DNA confinement in nanochannels: physics and biological applications. *Rep. Prog. Phys.* 75:106601.

21. Frykholm, K., L. K. Nyberg, and F. Westerlund, 2017. Exploring DNA–protein interactions on the single DNA molecule level using nanofluidic tools. *Integr. Biol.* 9:650–661.

22. Müller, V., and F. Westerlund, 2017. Optical DNA mapping in nanofluidic devices: principles and applications. *Lab Chip* 17:579–590.

23. Yadav, I., R. Basak, P. Yan, J. A. van Kan, V. Arluison, and J. R. C. van der Maarel, 2020. Role of Internal DNA Motion on the Mobility of a Nucleoid Associated Protein. *J. Phys. Chem. Lett.* 11:8424–8429.

24. Matsuoka, T., B. C. Kim, J. Huang, N. J. Douville, M. Thouless, and S. Takayama, 2012. Nanoscale squeezing in elastomeric nanochannels for single chromatin linearization. *Nano Lett.* 12:6480–6484.

25. Aguilar, C. A., and H. G. Craighead, 2013. Micro-and nanoscale devices for the investigation of epigenetics and chromatin dynamics. *Nat. Nanotechnol.* 8:709.

26. Streng, D. E., S. F. Lim, J. Pan, A. Karpusenka, and R. Riehn, 2009. Stretching chromatin through confinement. *Lab Chip* 9:2772–2774.

27. Yadav, I., W. Rosencrans, R. Basak, J. A. van Kan, and J. R. C. van der Maarel, 2020. Intramolecular dynamics of dsDNA confined to a quasi-one-dimensional nanochannel. *Phys. Rev. Research* 2:013294.

28. Wachsmuth, M., T. A. Knoch, and K. Rippe, 2016. Dynamic properties of independent chromatin domains measured by correlation spectroscopy in living cells. *Epigenet. Chromatin* 9:57.

29. Chubb, J. R., and T. B. Liverpool, 2010. Bursts and pulses: insights from single cell studies into transcriptional mechanisms. *Curr. Opin. Genet. Dev.* 20:478–484.

30. Berezhnoy, N. V., D. Lundberg, N. Korolev, C. Lu, J. Yan, M. Miguel, B. Lindman, and L. Nordenskiöld, 2012. Supramolecular organization in self-assembly of chromatin and cationic lipid bilayers is controlled by membrane charge density. *Biomacromolecules* 13:4146–4157.

31. Dorigo, B., T. Schalch, K. Bystricky, and T. J. Richmond, 2003. Chromatin fiber folding: requirement for the histone H4 N-terminal tail. *J. Mol. Biol.* 327:85–96.

32. Huynh, V. A., P. J. Robinson, and D. Rhodes, 2005. A method for the in vitro reconstitution of a defined 30 nm chromatin fibre containing stoichiometric amounts of the linker histone. *J. Mol. Biol.* 345:957–968.

33. van Kan, J. A., A. A. Bettiol, and F. Watt, 2006. Proton beam writing of three-dimensional nanostructures in hydrogen silsesquioxane. *Nano Lett.* 6:579–582.

34. Zhang, C., F. Zhang, J. A. van Kan, and J. R. C. van der Maarel, 2008. Effects of electrostatic screening on the conformation of single DNA molecules confined in a nanochannel. *J. Chem. Phys.* 128:225109.

35. van Kan, J. A., C. Zhang, P. P. Malar, and J. R. C. van der Maarel, 2012. High throughput fabrication of disposable nanofluidic lab-on-chip devices for single molecule studies. *Biomicrofluidics* 6:036502.

36. McMurray, C. T., and K. E. van Holde, 1986. Binding of ethidium bromide causes dissociation of the nucleosome core particle. *Proc. Natl. Acad. Sci. U. S. A.* 83:8472–8476.

37. Ladoux, B., J.-P. Quivy, P. Doyle, O. d. Roure, G. Almouzni, and J.-L. Viovy, 2000. Fast kinetics of chromatin assembly revealed by single-molecule videomicroscopy and scanning force microscopy. *Proc. Natl. Acad. Sci. U. S. A.* 97:14251–14256.

38. Kundukad, B., J. Yan, and P. Doyle, 2014. Effect of YOYO-1 on the mechanical properties of DNA. *Soft Matter* 10:9721–9728.

39. Dai, L., C. B. Renner, and P. S. Doyle, 2016. The polymer physics of single DNA confined in nanochannels. *Adv. Colloid Interface Sci.* 232:80–100.

40. Odijk, T., 1983. The statistics and dynamics of confined or entangled stiff polymers. *Macromolecules* 16:1340–1344.

41. Odijk, T., 2008. Scaling theory of DNA confined in nanochannels and nanoslits. *Phys. Rev. E* 77:060901.

42. Dai, L., S. Y. Ng, P. S. Doyle, and J. R. C. van der Maarel, 2012. Conformation model of back-folding and looping of a single DNA molecule confined inside a nanochannel. *ACS Macro Lett.* 1:1046–1050.

43. Muralidhar, A., D. R. Tree, and K. D. Dorfman, 2014. Backfolding of Wormlike Chains Confined in Nanochannels. *Macromolecules* 47:8446–8458.

44. Gelbart, W. M., R. F. Bruinsma, P. A. Pincus, and V. A. Parsegian, 2000. DNA-inspired electrostatics. *Phys. Today* 53:38–45.

45. Pegado, L., B. Jönsson, and H. Wennerström, 2016. Attractive ion–ion correlation forces and the dielectric approximation. *Adv. Colloid Interface Sci.* 232:1–8.

46. Korolev, N., A. Allahverdi, A. P. Lyubartsev, and L. Nordenskiöld, 2012. The polyelectrolyte properties of chromatin. *Soft Matter* 8:9322–9333.

47. Daoud, M., and P. G. de Gennes, 1977. Statistics of macromolecular solutions trapped in small pores. *J. Phys. (Paris)* 38:85–93.

48. De Gennes, P.-G., 1967. Quasi-elastic scattering of neutrons by dilute polymer solutions: I. Free-draining limit. *Phys. Phys. Fiz.* 3:37.

49. Doi, M., and S. F. Edwards, 1988. The theory of polymer dynamics, volume 73. Oxford University Press.

50. Lim, S. F., A. Karpusenko, A. L. Blumers, D. E. Streng, and R. Riehn, 2013. Chromatin modification mapping in nanochannels. *Biomicrofluidics* 7:064105.

51. Gruszka, D. T., S. Xie, H. Kimura, and H. Yardimci, 2020. Single-molecule imaging reveals control of parental histone recycling by free histones during DNA replication. *Sci. Adv.* 6:eabc0330.

SUPPLEMENTARY MATERIAL

An online supplement to this article can be found by visiting BJ Online at http://www.biophysj.org.